Optimization of LBNF Support Modules

Nicola Solieri*

University of Pisa

October 11, 2016

*E-mail: nicola.solieri@gmail.com

1 Introduction

The global neutrino physics community is developing a multi-decade physics program to measure unknown parameters of the Standard Model of particle physics and search for new phenomena. The program will be carried out as an international, leading-edge, dual-site experiment for neutrino science and proton decay studies, which is known as the Deep Underground Neutrino Experiment (DUNE). The detectors for this experiment will be designed, built, commissioned and operated by the international DUNE Collaboration. The facility required to support this experiment, the Long-Baseline Neutrino Facility (LBNF), is hosted by Fermilab and its design and construction is organized as a DOE/Fermilab project incorporating international partners. Together LBNF and DUNE will comprise the world's highest-intensity neutrino beam at Fermilab, in Batavia, IL, a high-precision near detector on the Fermilab site, a massive liquid argon time-projection chamber (LArTPC) far detector installed deep underground at the Sanford Underground Research Facility (SURF) 1300 km away in Lead, SD, and all of the conventional and technical facilities necessary to support the beamline and detector systems.

1.1 The beamline

The beamline is designed to provide a neutrino beam of sufficient intensity and appropriate energy range to meet the goals of DUNE for long-baseline neutrino oscillation physics. The design is a conventional, horn-focused neutrino beamline. The components of the beamline are designed to extract a proton beam from the Fermilab Main Injector and transport it to a target area where the collisions generate a beam of charged particles which decay into neutrinos to create the neutrino beam aimed at the near and far detectors.

The facility is designed for initial operation at proton-beam power of 1.2 MW, with the capability to support an upgrade to 2.4 MW. The plan is for twenty years of operation, while the lifetime of the Beamline Facility, including the shielding, is for thirty years. The conservative assumption is that for the first five years will be at 1.2 MW operations and the remaining fifteen years at 2.4 MW.

The experience gained from the various neutrino projects has been employed extensively in the reference design. In particular, the Neutrinos at the Main Injector (NuMI) beamline serves as the prototype design.

A proton-beam pulse from the primary-beam system enters the neutrino beamline system (from the right in through a beryllium "window." This window seals off the evacuated beam pipe of the primary beamline, and the protons enter the air-filled target chase (the volume surrounding the target and focusing system). Initially they pass through a small aperture in a 1.5-m-long graphite cylinder, called a baffle, which protects equipment downstream from mis-steered beam. Sixty-eight cm past the end of the baffle, they reach the target, a long, thin set of graphite segments in which about 85% of the protons interact and produce secondary particles. The target is partially surrounded by the first horn, a magnetized structure which provides initial focusing for the secondary particles, predominantly pions and kaons. A second horn, a few meters downstream, provides additional focusing for the secondary particles before they enter a He-filled 194 m long decay pipe, where a large fraction of the pions will decay to neutrinos, forming the neutrino beam. Horns are supported and positioned by support modules. Space is provided between the end of the second horn and the beginning of the decay pipe to allow flexibility for more advanced target-horn systems or ones optimized for different physics goals that may become relevant during the multi-decade lifetime of this facility. The final portion of the neutrino beamline is the absorber, downstream of the decay pipe. The absorber stops the protons that failed to interact in the target and the secondary particles that failed to decay to neutrinos; it is designed to sustain the beam energy deposition under expected normal operational conditions as well as under accident situations.

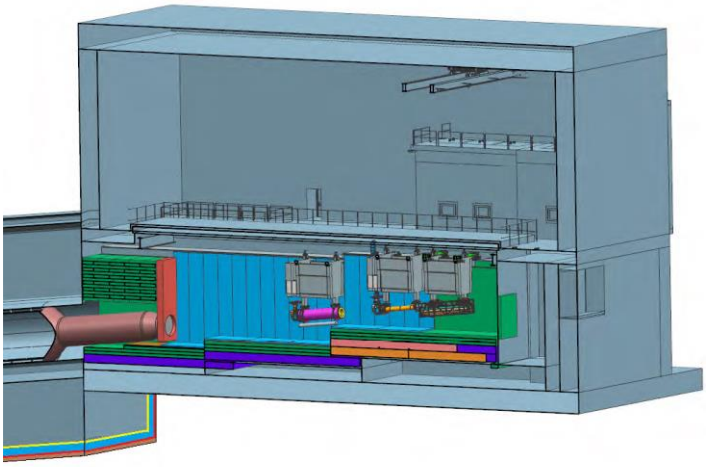

Figure 1 Schematic of the upstream portion of the LBNF neutrino beamline showing the major components of the neutrino beam. The target chase bulk steel shielding is shown mainly in green. Inside the target chase from right to left (the direction of the beam) pointing downwards: the beam window, horn-protection baffle, target, the two toroidal focusing horns mounted on their respective support modules and the decay pipe. At the upstream end of the decay pipe is a "snout" which holds the upstream decay pipe window. Above the chase and to the right is the work cell for horn and target system repairs. The grey areas around the decay pipe indicate concrete shielding. The yellow and red lines indicate multi-ply geosynthetic barriers, separated by a drainage layer (blue).

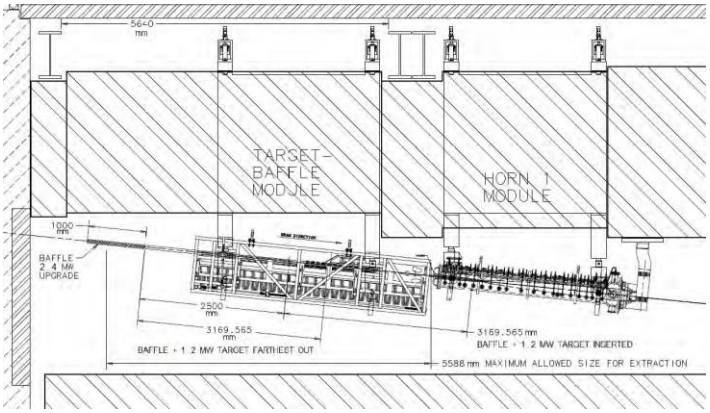

Figure 2 Target module in target pile shielding

1.1.1 Magnetic horns

The horns are focusing and sign selecting devices for secondary particles produced by the interaction of the primary proton beam on the target. This focusing of particles is achieved through a pulsed toroidal magnetic field, which is present in the inert gas volume between the co-axial inner and outer conductors that form the horn structure. The horns are identical to those developed for the NuMI neutrino beam, but they will be operated at 230 kA current and subjected to a beam power of 1.2 MW.

2 Horn support modules design

Horns will be supported and positioned by support modules.

The modules fix the horn with respect to the module in the horizontal degrees of freedom, but not in the vertical. The module is adjusted with respect to the beam for transverse horizontal position and yaw. The horn is adjusted with respect to the module for vertical and pitch alignment.

These components are crucial to the correct functioning of the beamline: not only do they provide a high degree of positioning accuracy (even under the intense heat load they experience when the beamline is operational), but the intensely radioactive environment present in the target chase requires that they also implement:

- Radiation shielding
- Remote control of horn position
- Remote connection and disconnection of feedthrough connections for the stripline, cooling water and instrumentation cabling from the top of the module mainframe, away from the most highly activated areas

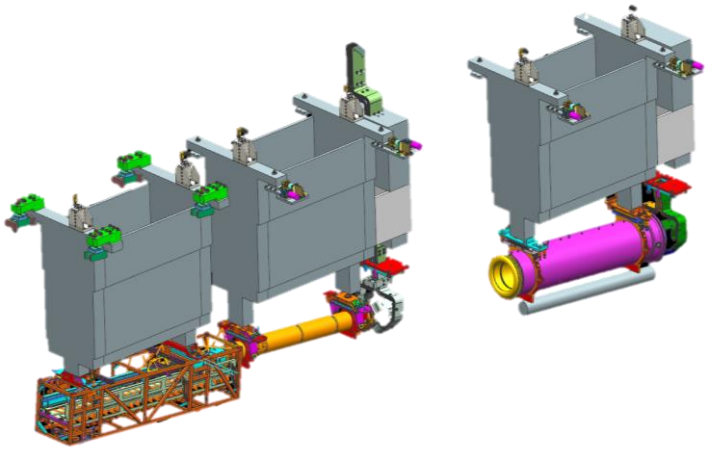

Figure 3 Target carrier, horn A and horn B and their support modules

Horn-support modules are rectangular boxes open at the top for shielding block insertion. They are constructed from plate steel, exception being made for every part that comes in contact with water, which is to be constructed from stainless steel, for the required corrosion resistance.

Unlike the majority of the components in the beamline, they have to be designed as "life of facility components", that is, they can't be replaced for the whole duration of the experiment.
Using an older module design for reference, the first step was redesigning all the different parts of the modules' mainframe using SIEMENS NX, making sure that they interfaced correctly with the target chase and the remote positioning mechanisms that had already been designed.

The result of this work can be seen in Figure 4.

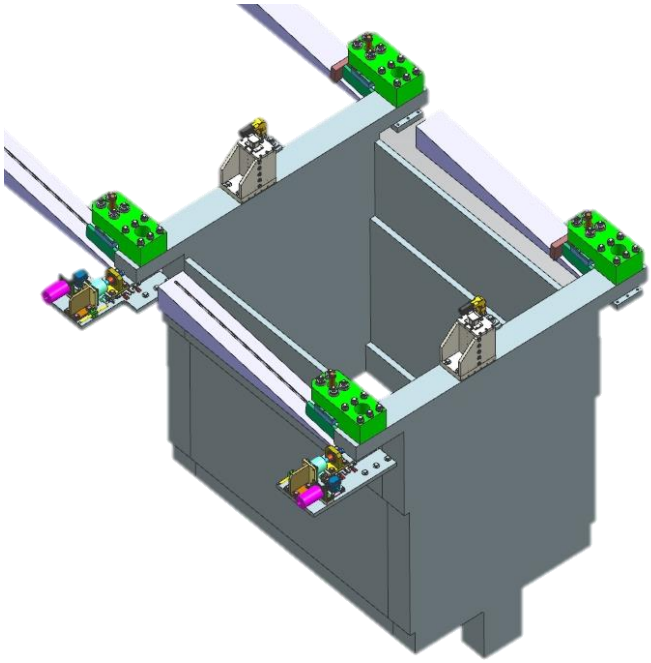

Figure 4 Module mainframe and remote positioning devices (on top)

The next step was designing the shielding blocks, using the NuMi module design for reference, as shown in Figure 5.

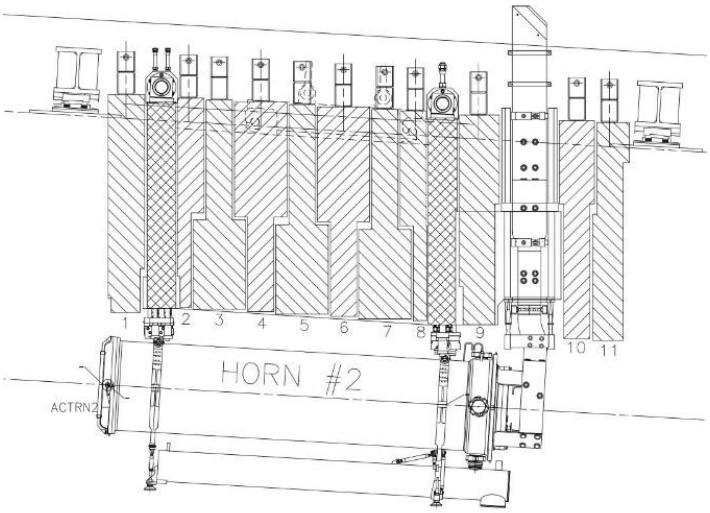

Figure 5 NuMi module design

In that design the shielding block, inserted in the module mainframe, is divided in a series of "T-blocks". There are two key advantages to this designs choice:

1. The single T-blocks are much lighter and easier to position in the module mainframe.
2. The surface area is vastly increased and so is heat dissipation

The shielding blocks have to be T-shaped in order to create a so called "labyrinth", which eliminates a clear line of sight from the bottom to the top of the module – a key requirement for radiation shielding.

Given the dimensions of the cavity present in the module mainframe and knowing that a ¾ inch lateral clearance is required for ease of handling and optimal heat dissipation, the number of blocks "n" was chosen as a compromise between radiation shielding and block temperature.

Intuitively, as n rises, the average block thickness decreases. This in turn leads to two conflicting phenomena:

- An increase in surface area causes better heat dissipation
- A decrease in block thickness reduces radiation shielding

After a few design iterations the best candidate for further analysis was found to be an assembly comprising five T-blocks, as shown in Figure 6.

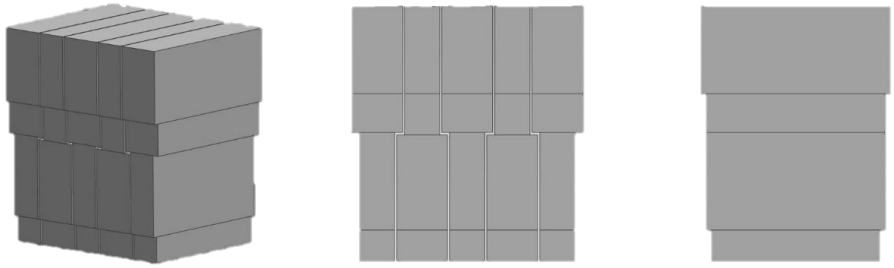

Figure 6 T-block assembly

Two block types are required to properly fit inside the module. The thickest part of the T-blocks measures 19.5 inches, whereas the thinnest measures 13.5. These dimensions yield a 3-inch step.

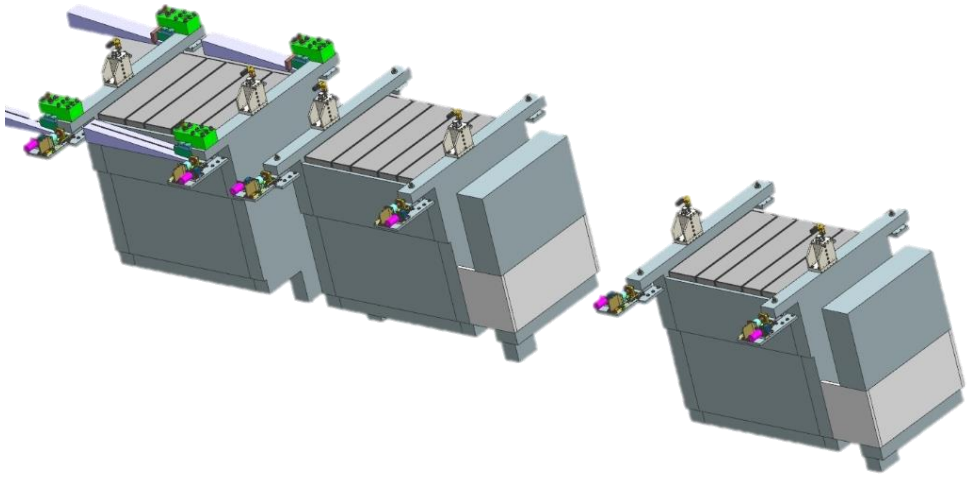

Figure 7 Module and T-block assembly

3 Finite Element Analysis of modules

The experience gained during the NuMi experiment shows that the known module concerns are temperature related, as thermal expansion and cooling affects the accuracy of horn positioning. All results presented in the following subsections are based on the MARS (a monte carlo code) modeling of the LBNF.

The modules were analyzed at all beam energies (60, 80 and 120GeV) to ensure life of facility design.

Three approaches were used in the analysis.

3.1 ANSYS Steady State Thermal

The first approach envisions the use of ANSYS Steady State Thermal.

After meshing the domain, the energy deposition (calculated by Fermilab's ES&H group using the MARS code) in the module mainframe and in the T-block assembly is modeled as a series of internal heat generation values in the different subdomains in which the model is divided.

The conversion is achieved using an excel sheet containing the energy deposition data, an energy deposition map detailing the different subdomains' positions and the following formula:

$$Heat\ gen.\left[{}^{W}/_{m^3}\right] = (En.Dep.\left[{}^{GeV}/_{g}\right]) * e * Protons\ per\ Cycle * \frac{1.0e9}{Cycle\ Time} * Density$$

Unfortunately ANSYS Steady State Thermal does not account for variations in air temperature. Since this simulation is performed merely to obtain a first estimate of module temperatures, the problem was ignored at this stage and was further analyzed in the following simulations.

Therefore, the effect of air convection was modeled using the "Convection" boundary condition present in ANSYS Steady State Thermal: after selecting all the exposed faces, the program requires the user to specify a heat transfer coefficient value and the ambient temperature, as shown in Figure 8.

Details of "Convection"

Scope	
Scoping Method	Geometry Selection
Geometry	192 Faces
Definition	
Type	Convection
Film Coefficient	10. W/m²·°C (ramped)
Ambient Temperature	22. °C (ramped)
Convection Matrix	Program Controlled
Suppressed	No

Figure 8 "Convection" boundary condition setup panel

The results of this simulation are shown in Figure 9

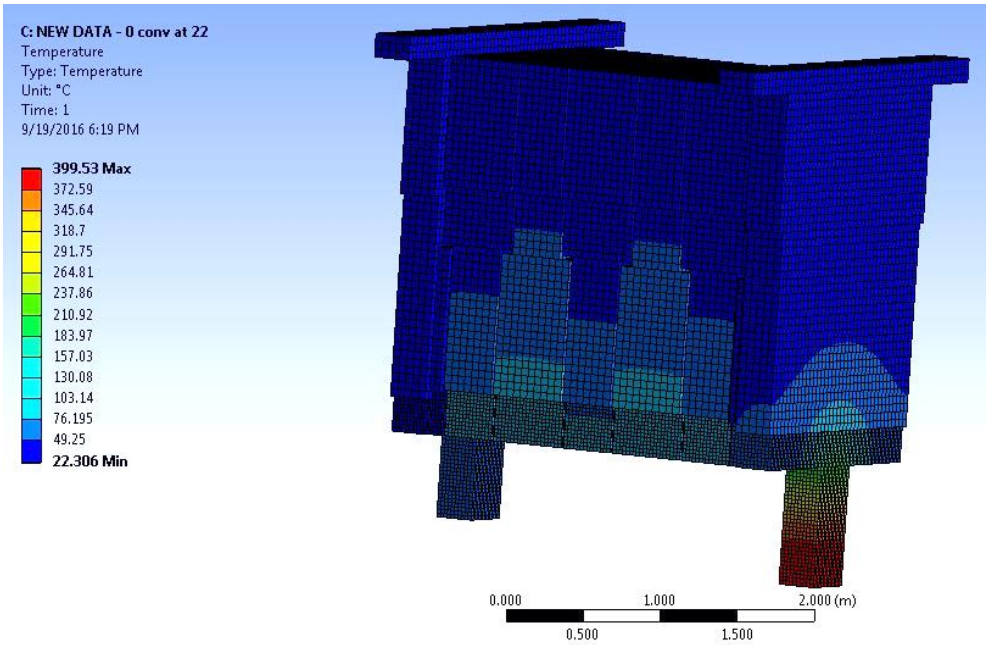

Figure 9 Steady State Thermal simulation

The simulation shows there are two areas to focus on:

- The T-block assembly
- The downstream endwall's stalactite

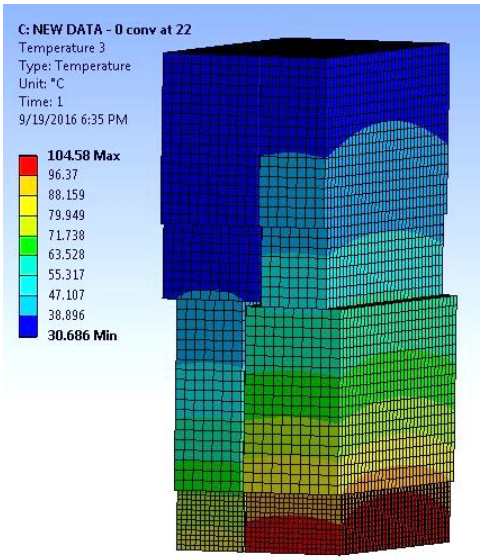

Figure 10 T-block assembly

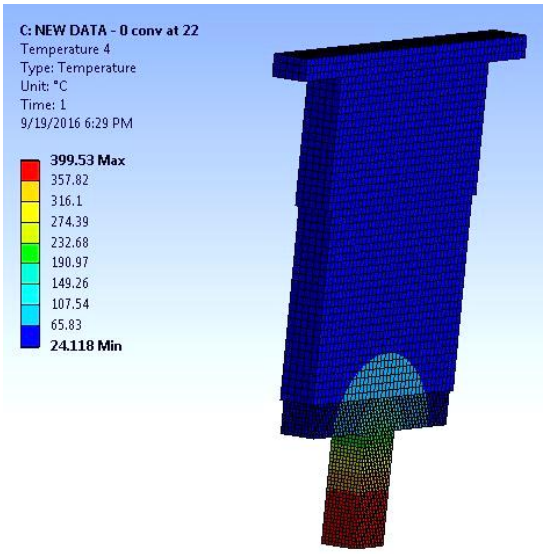

Figure 11 Downstream endwall's stalactite

3.2 Steady State Thermal + Fluent iteration

This approach was developed in an effort to obtain a first evaluation of the effect of the temperature of the air present in the gap on the model.

The process is iterative: a single simulation cycle is divided into four substeps

1. The ANSYS Steady State Thermal analysis is used as the starting point.
2. After choosing the central T-block couple, the Steady State Thermal conceptual temperatures along the edges are used as boundary conditions in a 2D CFD simulation performed using ANSYS Fluent.
3. Ambient temperature values are layered in ANSYS Steady State Thermal accordingly.
4. A new Steady State Thermal Analysis is performed.

The amount of simulation cycles to be performed is entirely up to the user's discretion. The suggested convergence criterium is:

$$[(Max\ Temperature)_{i+1} - (Max\ Temperature)_i] < 5°C$$

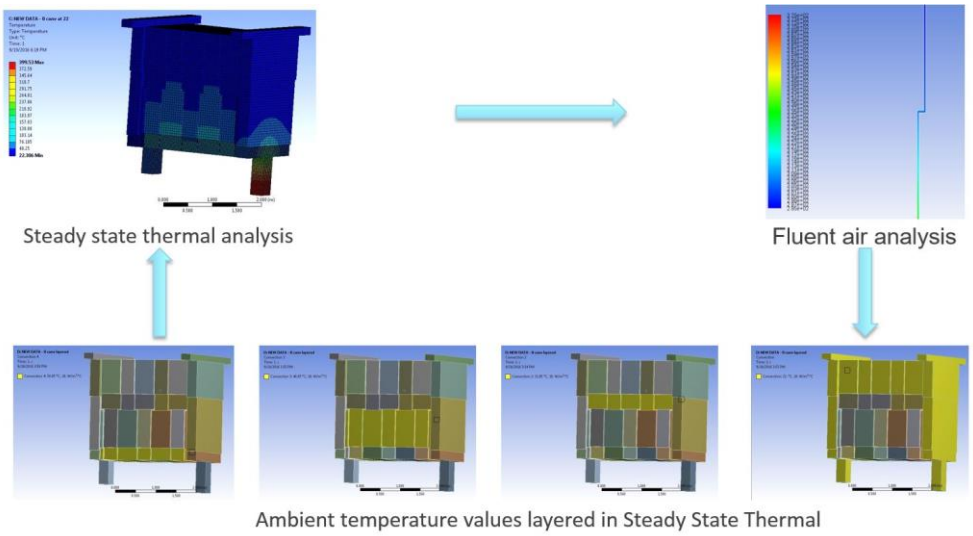

Figure 12 A single iteration cycle

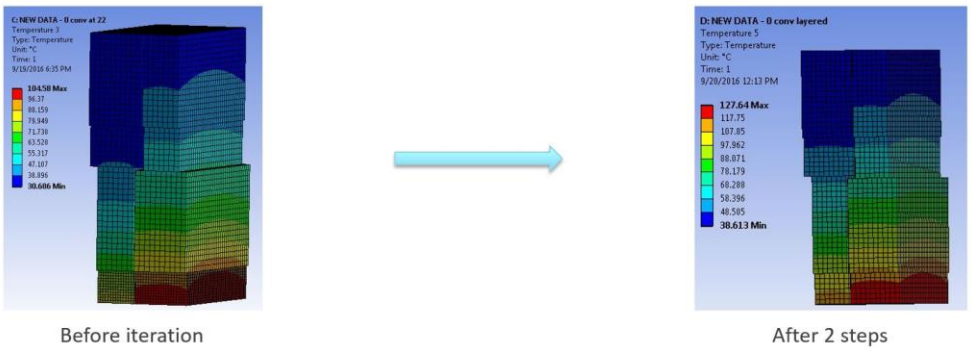

Figure 13 After two cycles, the maximum conceptual temperature in the blocks rises by 23°C

As expected, air state is a key factor: a better model is required.

3.3 2D Fluent analysis

The key assumption underlying this is simulation is that, since the blocks' width is more than five times their average thickness, a 2D simulation using ANSYS Fluent is both phisically accurate and conservative.

The benefits of such a simulation are:

- The model is comprehensive: it simultaneously analyzes conduction within the metal and airflow in the gaps (two separate aspects in the previously introduced simulations)
- The resulting analysis is more accurate

- The model is further simplified using appropriate simmetries. From a computational standpoint, the simulation is extremely light.

Many aspects of the problem can be simultaneously analyzed once the simulation has converged:

- T-block temperature
- Airflow properties: there are several interesting properties to evaluate, the main interesting of which is verifying the absence of airflow reversal.

  Since air is fed from the top of the module and T-blocks are hotter at the bottom, it is necessary to verify that inlet velocity is high enough to avoid airflow reversal, which would prevent some parts of the blocks from having a fresh flow of air along their edge.
- Effect of boundary condition variations, such as the one analyzed in the next paragraph.

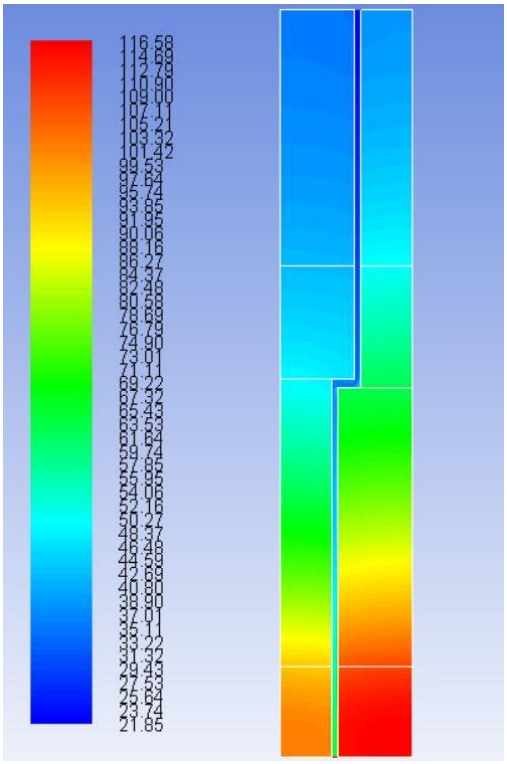

Figure 14 Contours of static temperature

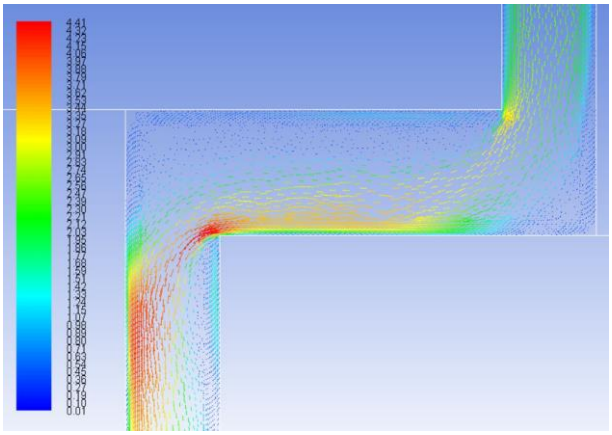

Figure 15 Air speed vectors, colored by velocity magnitude

3.3.1. Effect of inlet velocity

The results presented so far have shown that air state is a key factor in the physics of this problem.

Since the simulation is so computationally light, the analysis of the effect of inlet speed variation on T-block temperature is rather effortless.

The graph below shows the maximum conceptual temperature in the blocks as a function of inlet speed in its expected range.

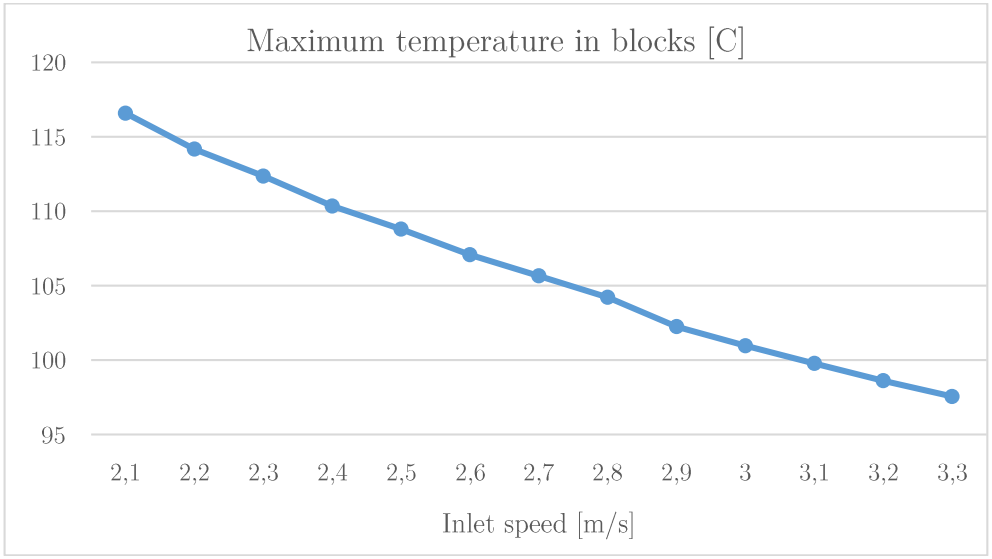

A 1.2 m/s difference in air speed yields a 20°C temperature difference, a definitive confirmation of the importance of air conditions in this problem.

3.4 Summary

Three methods have now been introduced to analyze the thermal behavior of any given T-block assembly:

- Steady state tempeature analysis
- Steady state + fluent iteration
- Fluent 2D analysis

It's important to keep in mind that each one has its own set of pros and cons: the first two simulations, for example, are easy to setup once the module and t-block assembly is ready and they provide a reasonably accurate temperature estimate.

The last simulation, while having a more time consuming setup, offers a more comprehensive and detailed look at the problem as well as an interesting set of tools, such as the aforementioned boundary condition variation approach.

A full 3D CFD analyis will be required in the final design stage to properly asses the control rod heat deformation: a key information required to properly determine the horn's displacement in operation.

4 Cold Plate

As mentioned above, the temperature reached in the stalagtite is too high. Since the control rod used to support and position the magnetic horns is inserted within the end walls and comes out of the bottom part of the stalactites, such a high temperature in that area heavily affects the accuracy of horn positioning during operation.

Heat has to be removed from that area: the obvious design choice is the installation of two cold plates on the stalactite's sides.

4.1 Design

Out of the geat variety of cold plate designs the attention was focused on the two most reliable ones:

- Formed Tube Cold Plate (FTCP).
  The coolant tubes are attached to the cold plate substrate by soldering or using a thermal epoxy. In this design, shown in Figure 16, a copper plate

is generally used, although aluminum is sometimes employed in lowpower applications. This is one of the simplest cold plate designs, but its performance is rather poor, limiting its use in the low-power applications.

Figure 16 Formed Tube Cold Plate (FTCP)

- Deep Drilled Cold Plate (DDCP)

  As the power dissipation increases, the contact resistance of the plate and the tube wall become unacceptably high. In this design, shown in Figure 17, deep holes are drilled in the plane of the substrate plate, generally made of copper. These holes are then configured with end caps (or plugs) to create coolant flow paths through the substrate.

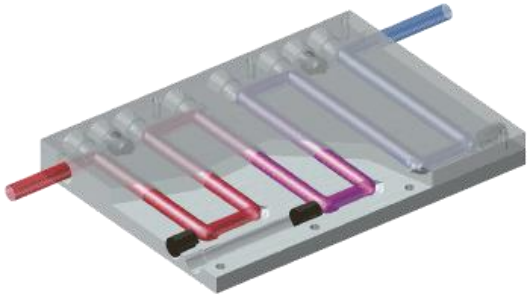

Figure 17 Deep Drilled Cold Plate

The better performances offered by the latter design and the possibility to manufacture the cold plates using the lab's mechanical workshop are the reason why the design and analysis efforts were focused on it.

A section view of the deep drilled cold plate that was designed and later analyzed is shown in Figure 18.

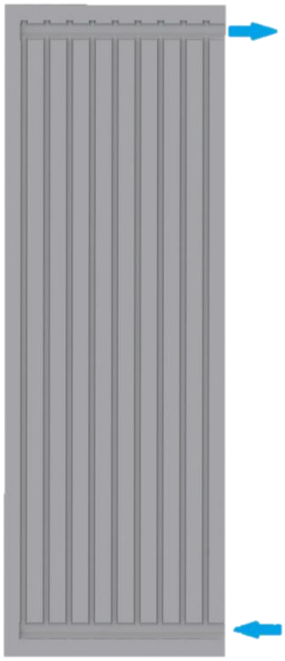

Figure 18 Conceptual cold plate design - section view

This design features two horizontal Φ 24 distribution channels and nine Φ 8 connection channels. Since the maximum conceptual temperatures registered in the stalactite are at its bottom, water is fed from the bottom to maximize ΔT.

In an effort to maximize heat exchange, the design is asymmetric: as shown in Figure 19, the vertical connection channels are placed closer to the side that will come in contact with the stalactite.

The presence of nitric acid in the Target Hall precludes the use of copper for the construction of the cold plate: the material chosen was aluminum, as a compromise between corrosion restistance and heat conductivity.

The cold plate was designed and tested for water glow rates between 10 and 40 $^{l}/_{min}$.

The stalactites are not the only components present in the Target Hall to be water cooled. Since these elements are operated in an environment with a high flux of energetic particles from the beam interacting with the target, the cooling water itself will be activated and cannot be allowed to mix with un-activated water. Therefore, these components are cooled using closed-circuit water system; the heat being moved by conduction and convection to secondary water heat-exchanger/chiller system connected to the outside world.

Figure 19 Welded plugs used to create a coolant path

Figure 20 Cold plate installed on the stalactite's side

4.2 Analysis

In order to determine the effectiveness of this design a 3D CFD analysis using ANSYS CFX was performed.

With this analysis it's possible to simultaneously analyze several aspects of the problem, such as:

- Water flow
- Temperature
- Effect of boundary condition variations

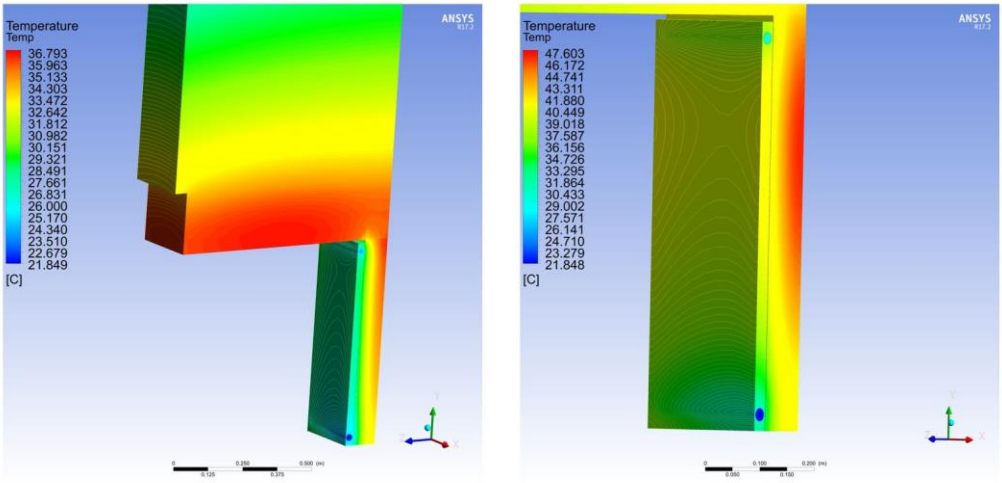

Figure 21 Details of one of the numerous performed simulations

The analysis was validated by comparing the simulated water ΔT with calculations by hand and by observing the absence of anomalies in water streamlines.

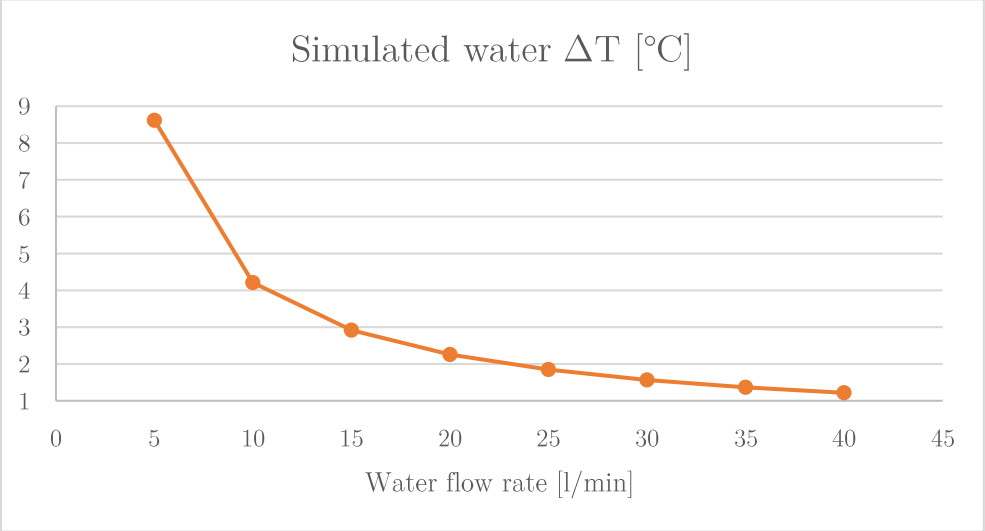

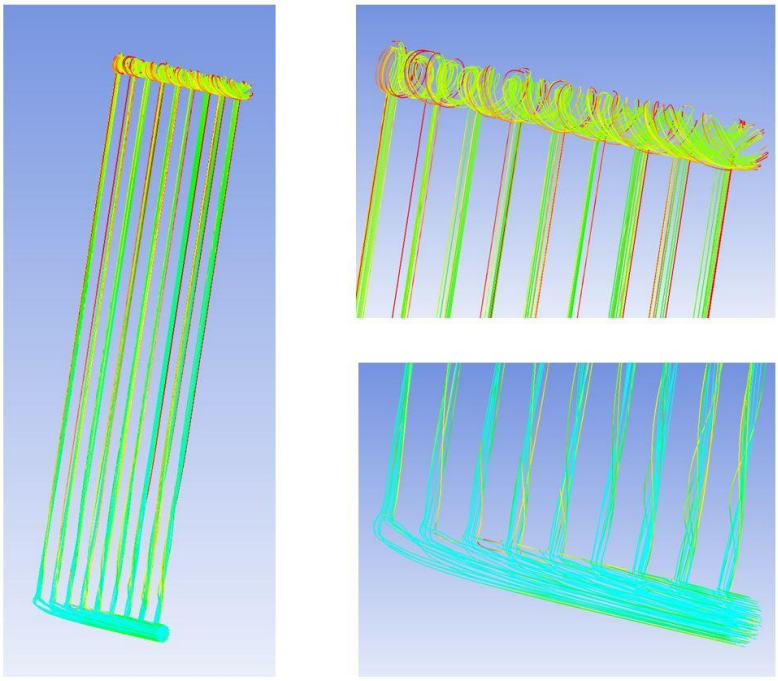

Figure 22 Water streamlines colored by temperature magnitude

Similarly to what had already been performed in the 2D analysis a boundary condition variation study was run.

The results are summarized in the next graph.

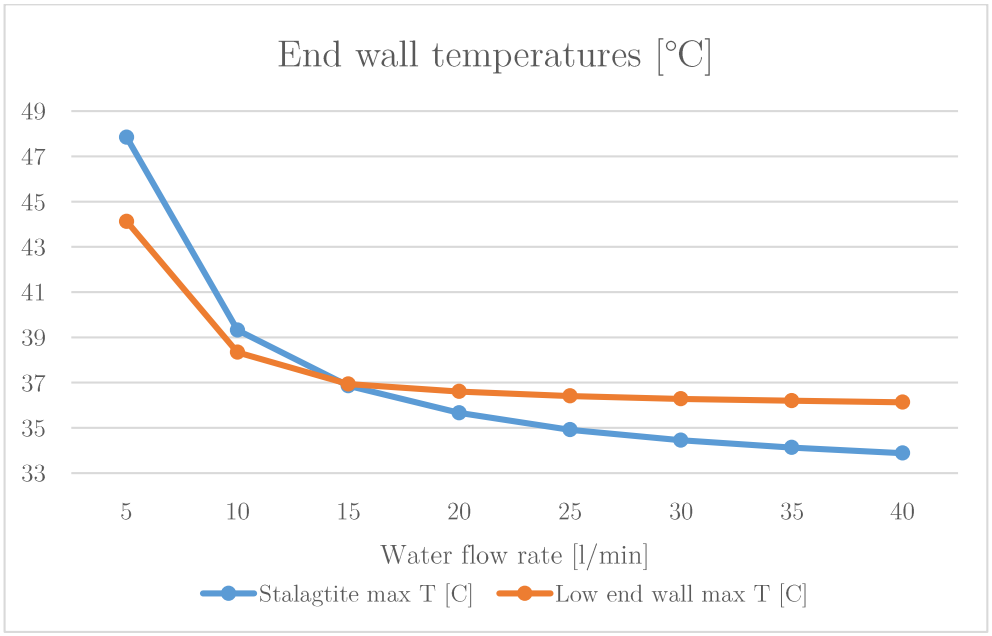

There are two aspects to consider:

1. Even at the lowest flow rate, the thermal performance of the cold plate is still excellent: the maximum temperature in the stalactite is decreased from 325°C to just 48°C.
2. A diminishing returns behavior was expected in this problem. In particular, increasing water flow rates over 15 $^{l}/_{min}$ (after this point the maximum temperature is found in the lower part of the end wall and no longer in the stalactite) is not justified by the incremental temperature reduction.

5 Module connection to horns

The horn is connected to the module through a couple of vertical invar rods inserted in the module end walls. This way the horn can be adjusted with respect to the module for vertical and pitch alignment.

Previous designs envisioned a threaded connection between the rod end and its housing in the horn.

This connection was often subject to galling, a phenomenon that made the connection difficult to reuse.

The new proposed design, shown in Figure 23, eliminates this problem. It expands upon the proven connection method used for stripline block attachment.

The vertical rod has a hole near its end in which is inserted a small horizontal rod that is held in place with a grub screw.

The working principle is simple: the control rod slides in the housing and then it's turned 90°. Once the control rod is lifted, the horizontal rod finds a matching cylindrical surface: at that point the connection is made.

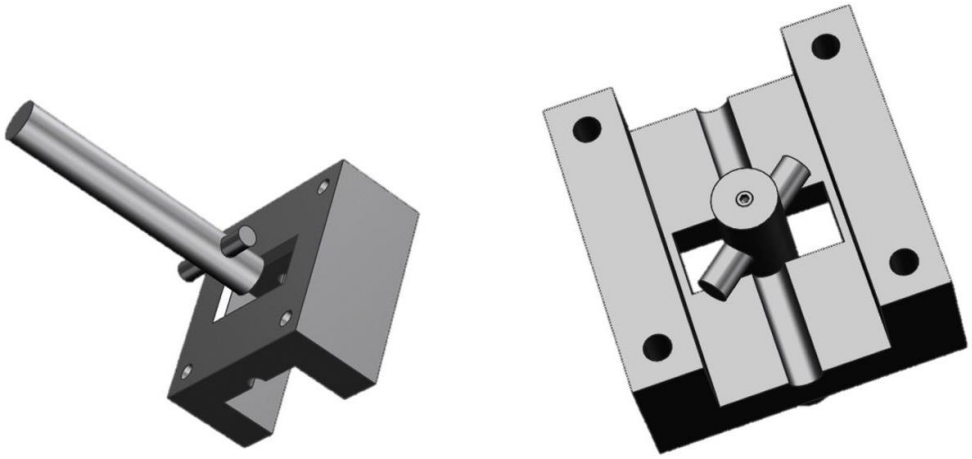

Figure 23 Connection mechanism's working principle

The mechanism was then analyzed using ANSYS Steady Structural. The results are shown in Figure 24.

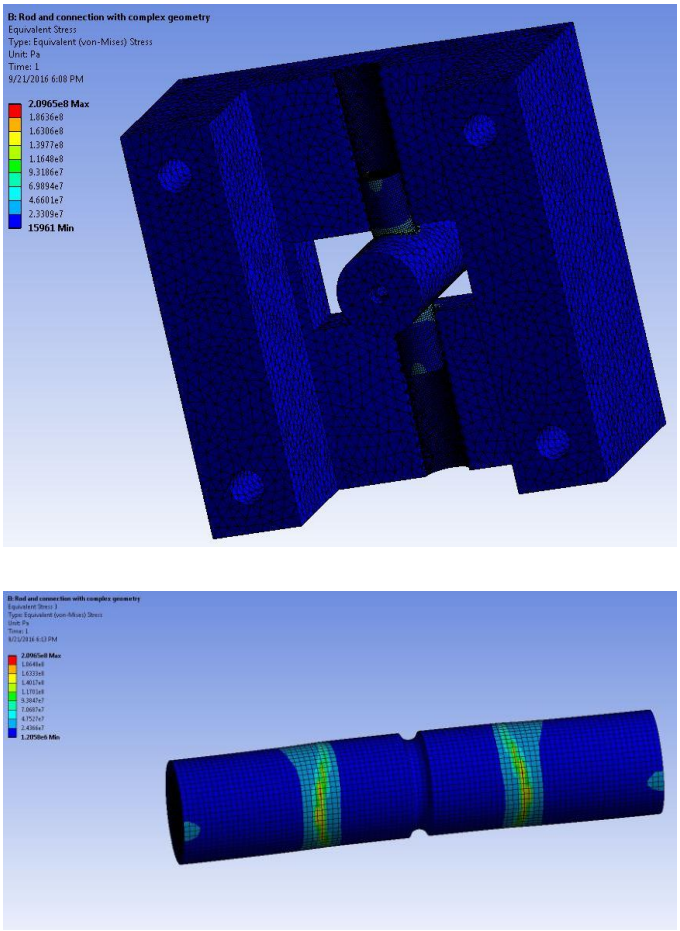

Figure 24 Steady Structural analysis of mechanism

The analysis highlights the presence of a 209 Mpa Von Mises equivalent stress peak in the horizontal rod, which yields a 2.5 safety factor.
The design is easily scalable if a higher safety factor is found to be required.

The upstream and downstream housings were subsequently redesigned in order to accept this new connection mechanism. The results of this process are shown in Figure 25, 26 and 27.

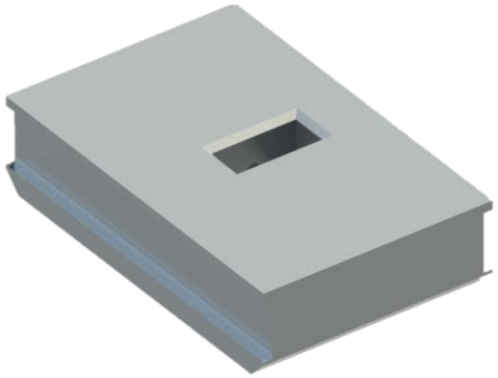

Figure 25 Upstream horn connection

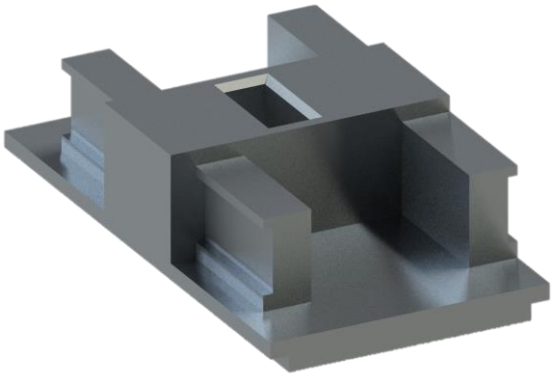

Figure 26 Downstream horn connection

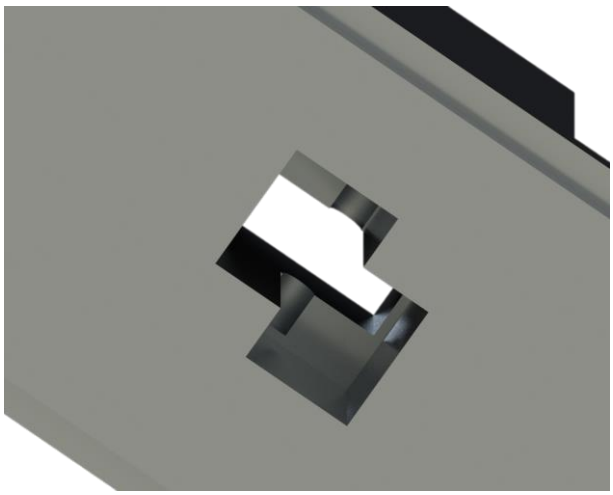

Figure 27 Turn stop implemented in the underside of the connection

The design can be modular.